

1 NEON Crowns: a remote sensing 2 derived dataset of 100 million individual 3 tree crowns

4 Ben. G. Weinstein¹ Sergio Marconi¹, Stephanie Bohlman², Alina Zare³, Aditya Singh⁴, Sarah J.
5 Graves⁵, Ethan White¹

6 ¹Department of Wildlife Ecology and Conservation, University of Florida, Gainesville, Florida,
7 USA

8 ²School of Forest Resources and Conservation, University of Florida, Gainesville, Florida, USA

9 ³Department of Electrical and Computer Engineering, University of Florida, Gainesville, Florida,
10 USA

11 ⁴Department of Agricultural & Biological Engineering, University of Florida, Gainesville, FL
12 32611, USA

13 ⁵Nelson Institute for Environmental Studies, University of Wisconsin-Madison, Madison,
14 Wisconsin, USA

15 Abstract

16 Forests provide essential biodiversity, ecosystem and economic services. Information on
17 individual trees is important for understanding the state of forest ecosystems but obtaining
18 individual-level data at broad scales is challenging due to the costs and logistics of data
19 collection. While advances in remote sensing techniques allow surveys of individual trees at
20 unprecedented extents, there remain significant technical and computational challenges in

21 turning sensor data into tangible information. Using deep learning methods, we produced an
22 open-source dataset of individual-level crown estimates for 100 million trees at 37 sites across
23 the United States surveyed by the National Ecological Observatory Network's Airborne
24 Observation Platform. Each canopy tree crown is represented by a rectangular bounding box
25 and includes information on the height, crown area, and spatial location of the tree. Tree crowns
26 identified using this technique correspond well with hand-labeled crowns, exhibiting both high
27 levels of overlap and good correspondence in height estimates. These data have the potential
28 to drive significant expansion of individual-level research on trees by facilitating both regional
29 analyses at scales of ~10,000 ha and cross-region comparisons encompassing forest types
30 from most of the United States.

31 Introduction

32 Trees are central organisms in maintaining the ecological function, biodiversity and the health of
33 the planet. There are estimated to be over three trillion individual trees on earth (Crowther et al.,
34 2015) covering a broad range of environments and geography (Hansen et al., 2013). Counting
35 and measuring trees is central to developing an understanding of key environmental and
36 economic issues and has implications for global climate, land management and wood
37 production. Field-based surveys of trees are generally conducted at local scales (~0.1-100 ha)
38 with measurements of attributes for individual trees within plots collected manually. Connecting
39 these local scale measurements at the plot level to broad scale patterns is challenging because
40 of spatial heterogeneity in forests. Many of the key processes in forests, including change in
41 forest structure and function in response to disturbances such as hurricanes and pest
42 outbreaks, and human modification through forest management and fire, occur at scales beyond
43 those feasible for direct field measurement.

44 Satellite data with continuous global coverage have been used to quantify important
45 patterns in forest ecology and management such as global tree cover dynamics and
46 disturbances in temperate forests (e.g. Bastin et al., 2018). However, the spatial resolution of
47 satellite data makes it difficult to detect and monitor individual trees that underlie large scale
48 patterns. These shortcomings can however be overcome by utilizing higher resolution remotely
49 sensed data from low Earth orbit satellites, aircraft or drones to capture individual-level changes
50 in forest structure and composition (Aubry-Kientz et al., 2019; Puliti et al., 2020). These high-
51 resolution data have become increasingly accessible but converting the data into information on
52 individual trees requires significant technical expertise and access to high-performance
53 computing environments. This prevents most ecologists, foresters, and managers from
54 engaging with large scale data on individual trees, despite the availability of the underlying data
55 products and broad importance for forest ecology and management.

56 In response to the growing need for publicly available and standardized airborne remote
57 sensing data over forested ecosystems, the National Ecological Observatory Network (NEON)
58 is collecting multi-sensor data for more than 40 sites across the US. In this research, we
59 combine these sensor data with a semi-supervised deep learning approach (Weinstein et al.,
60 2020b, 2019) to produce a dataset on the location, height and crown area of over 100 million
61 individual canopy trees at 37 sites distributed across the United States. To make these data
62 readily accessible, we are releasing easy to access data files to spur biological analyses and to
63 facilitate model development for tasks that rely on individual tree prediction. We describe the
64 components of this open-source dataset, compare predicted crowns with hand-labeled crowns
65 for a range of forest types, and discuss how this dataset can be used to address key questions
66 in forest research.

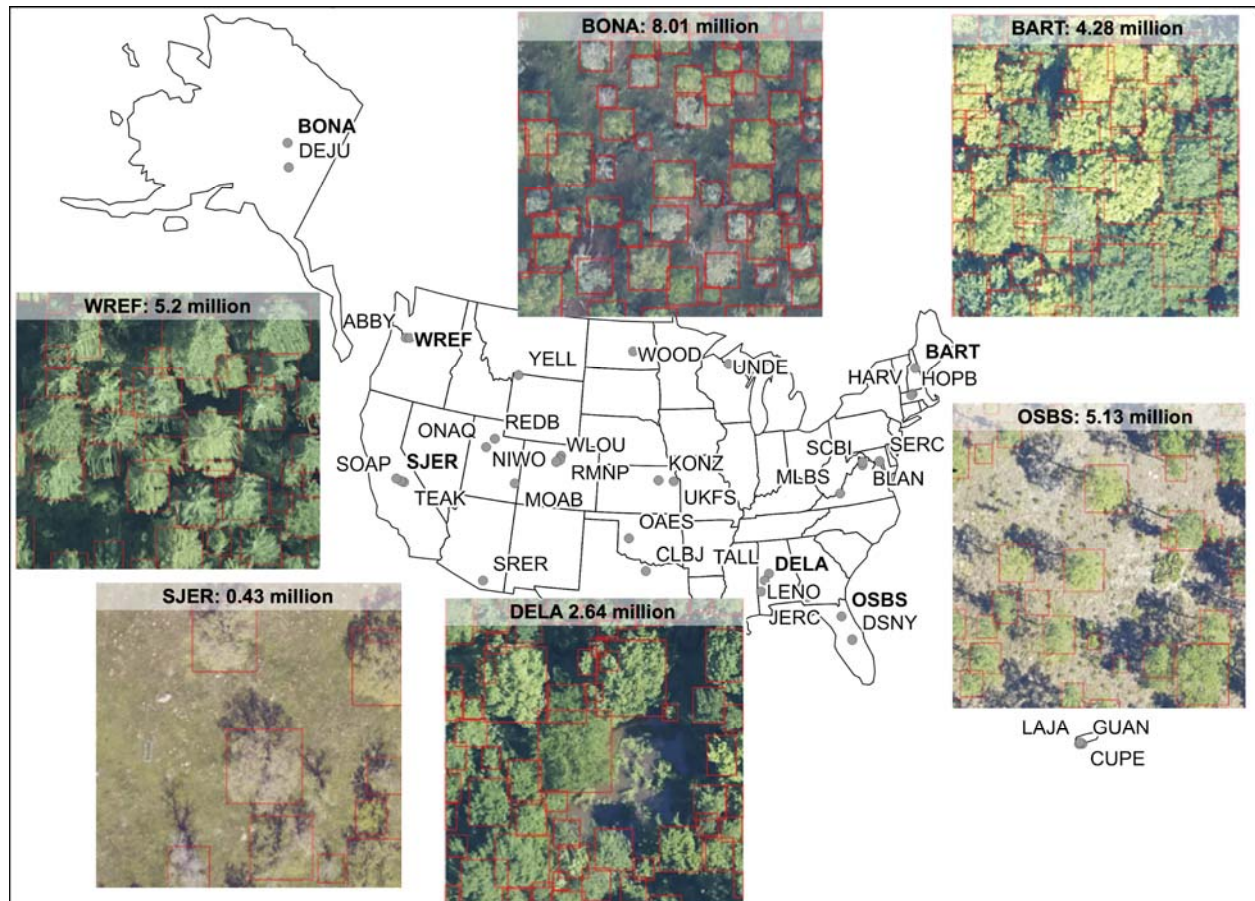
67 The NEON Crowns dataset

68 The NEON Crowns dataset contains tree crowns for all canopy trees (those visible from
69 airborne remote sensing) at 37 NEON sites. Since subcanopy trees are not visible from above,
70 they are not included in this dataset. We operationally define “trees” as plants over 3m tall. The
71 37 NEON sites represent all NEON sites containing trees with co-registered RGB and LiDAR
72 data from 2018 or 2019 (see S3 for a list of sites and their locations). Predictions were made
73 using the most recent year for which images were available for each site.

74 The dataset includes a total of 104,675,304 million crowns. Each predicted crown
75 includes data on the spatial position of the crown bounding box, the area of the bounding box
76 (an approximation of crown area), the 99th quantile of the height of LiDAR returns within the
77 bounding box above ground level (an estimate of tree height), the year of sampling, the site
78 where the tree is located, and a confidence score indicating the model confidence that the box
79 represents a tree. The confidence score can vary from 0-1, but based on results from
80 (Weinstein et al., 2020b), boxes with less than 0.15 confidence were not included in the dataset.

81 The dataset is provided in two formats: 1) as 11,000 individual files each covering a
82 single 1km² tile (geospatial ‘shapefiles’ in standard ESRI™ format); and 2) as 37 csv files,
83 each covering an entire NEON site. Geospatial tiles have embedded spatial projection
84 information and can be read in commonly available GIS software (e.g., ArcGIS, QGIS) and
85 geospatial packages for most common programming languages used in data analysis (e.g., R,
86 Python). All data are publicly available, openly licensed (CC-BY), and permanently archived on
87 Zenodo (<https://zenodo.org/deposit/3765872>).

88

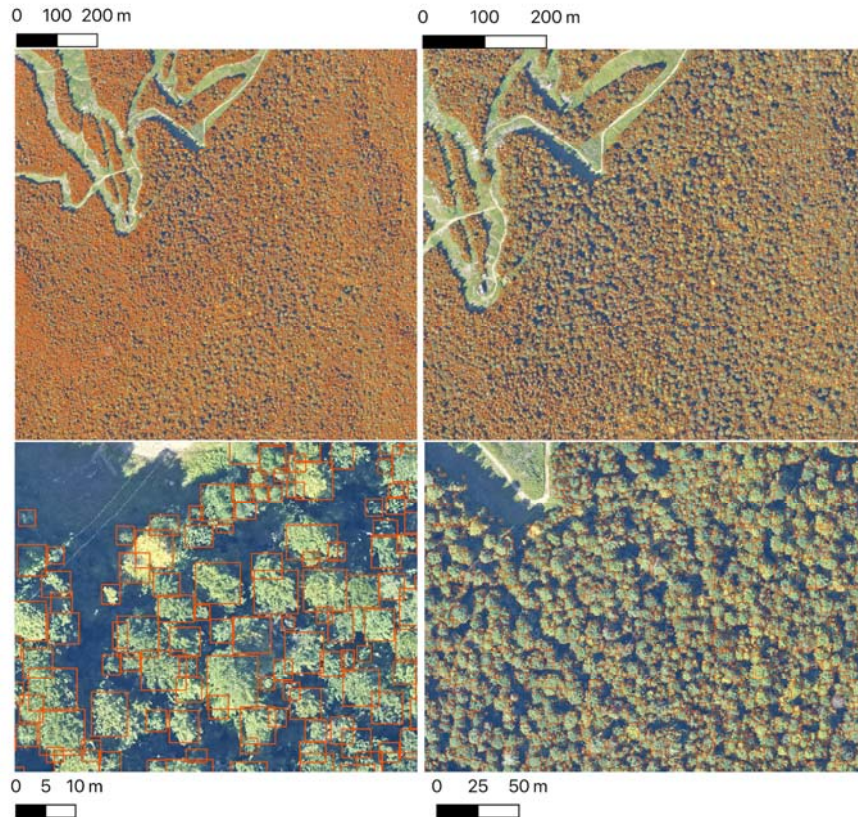


89

90 Figure 1. Locations of 37 NEON sites included in the NEON Crowns Dataset and examples of
91 tree predictions shown with RGB imagery for six sites. Clockwise from bottom right: 1) OSBS:
92 Ordway-Swisher Biological Station, Florida 2) DELA: Dead Lake, Alabama, 3) SJER: San
93 Joaquin Experimental Range, California, 4) WREF: Wind River Experimental Forest,
94 Washington, 5) BONA: Caribou Creek, Alaska and 6) BART: Bartlett Experimental Forest, New
95 Hampshire. Each predicted crown is associated with the spatial position, crown area, maximum
96 height estimate from co-registered LiDAR data, and a predicted confidence score.

97 To support the visualization of the dataset we have developed a web visualization tool using
98 the ViSUS WebViewer (www.visus.org) to allow users to view all of the trees at the full site scale

99 with the ability to zoom and pan to examine individual groups of trees down to a scale of 20m
100 (see <http://visualize.idtrees.org>, Figure 2). This tool will allow the ecological community to assist
101 in identifying areas in need of further refinement within large area covered by the 37 sites.

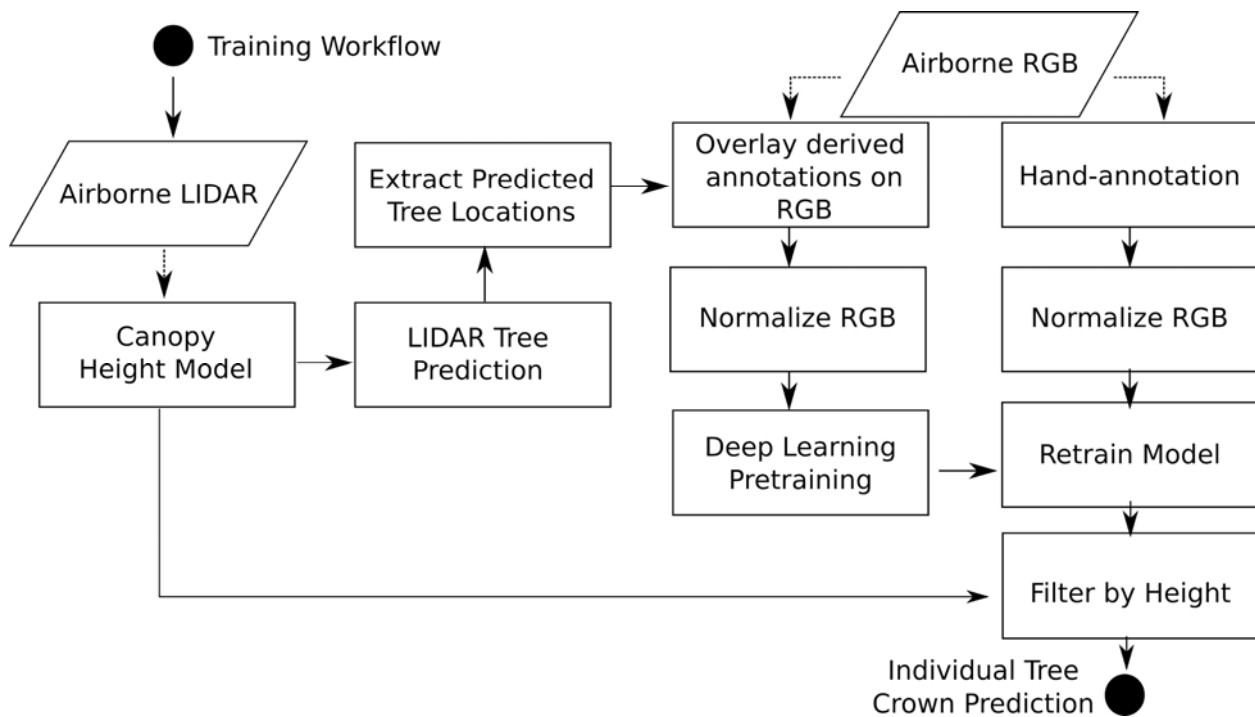


102
103 Figure 2. The Neon Crowns Dataset provides individual-level tree predictions at broad scales.
104 An example from Bartlett Forest, NH shows the ability to continuously zoom from landscape
105 level to stand level views. A single 1km tile is shown. NEON sites tend to have between 100 to
106 400 tiles in the full airborne footprint.

107 Crown Delineation Methods

108 The location of individual tree crowns was estimated using a semi-supervised deep learning
109 workflow (Figure 3; Weinstein et al., 2020b, 2019). This workflow uses a one-shot object

110 detector with a convolutional neural network backbone to identify trees in RGB imagery. The
111 model was pre-trained using weak labels generated from a previous published LiDAR tree
112 detection algorithm using NEON data from 30 sites (Silva et al., 2016). The model was then
113 trained on 10,000 hand-annotated crowns from 7 NEON sites (Figure 1). This phase of the
114 workflow was performed using the DeepForest python package (Weinstein et al., 2020a). We
115 extend the workflow by filtering trees using the LiDAR-derived canopy height model to remove
116 objects identified by the model with heights of <3m (Supplementary Material). This addition was
117 important in sparsely vegetated landscapes, such as oak savannah and deserts where it was
118 difficult for the model to distinguish between trees and low shrubs in the RGB imagery.
119



120

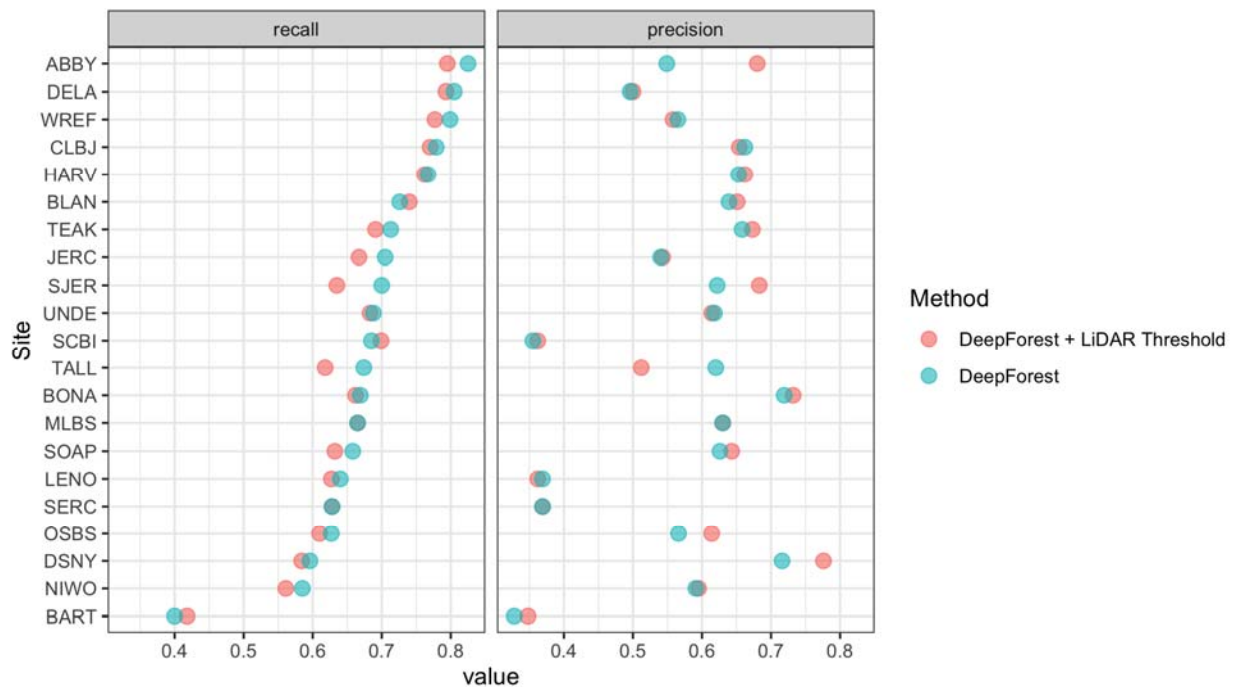
121 Figure 3. Workflow diagram adapted from (Weinstein et al., 2020a). The workflow for model
122 training and development are identical to (Weinstein et al., 2020a) with the exception of
123 extracting heights from the canopy height model for each bounding box prediction.

124 Evaluation and Validation

125 Building on evaluation methods from Weinstein et al., (2020b, 2020a, 2019), we validated the
126 dataset using hand-annotated bounding boxes drawn by an observer looking directly at the
127 sensor data. We refer to this type of evaluation data as ‘image-annotated crowns’. This
128 approach allows the performance of the crown-delineation algorithm to be evaluated across the
129 full range of forest types represented in the continental-scale dataset. However, note that these
130 image-annotated crowns will not be as accurate as field-annotated crowns (S. Graves et al.,
131 2018), where an observer records crown position while physically next to the target tree. Image-
132 annotated crowns may therefore overestimate the performance of the algorithm relative to more
133 precise ground truth.

134 We compared predicted tree crowns to image-annotated crowns from 21 NEON sites
135 (n=207 images, 6926 trees) that were withheld from model training. These sites were selected
136 to cover a wide range of forest types and geographies. Using a 50% intersection over union
137 threshold, our workflow yielded a bounding box recall of 72.4% with a precision of 70.5%. Recall
138 is the proportion of image-annotated crowns matched to a crown prediction and precision is the
139 proportion of predictions that match image-annotated crowns. Precision and recall are equally
140 important for developing a tree crown dataset, because it is important to both successfully
141 identify trees and ignore non-tree objects. Tests indicate that the model generalizes well across
142 geographic sites and forest conditions (Figure 4; Weinstein et al., 2020a, 2020b), but there is a
143 general bias towards undersegmenting trees in dense stands where multiple individual trees
144 with similar optical characteristics are grouped into a single delineation. Additional training data
145 and the LiDAR threshold added in this implementation resulted in predictions that were 4.1%
146 more precise, but 2.8% less accurate than (Weinstein et al., 2020a) (Figure 4). The decrease in
147 recall likely occurs because the NEON field plots that were used for evaluation occur mostly in

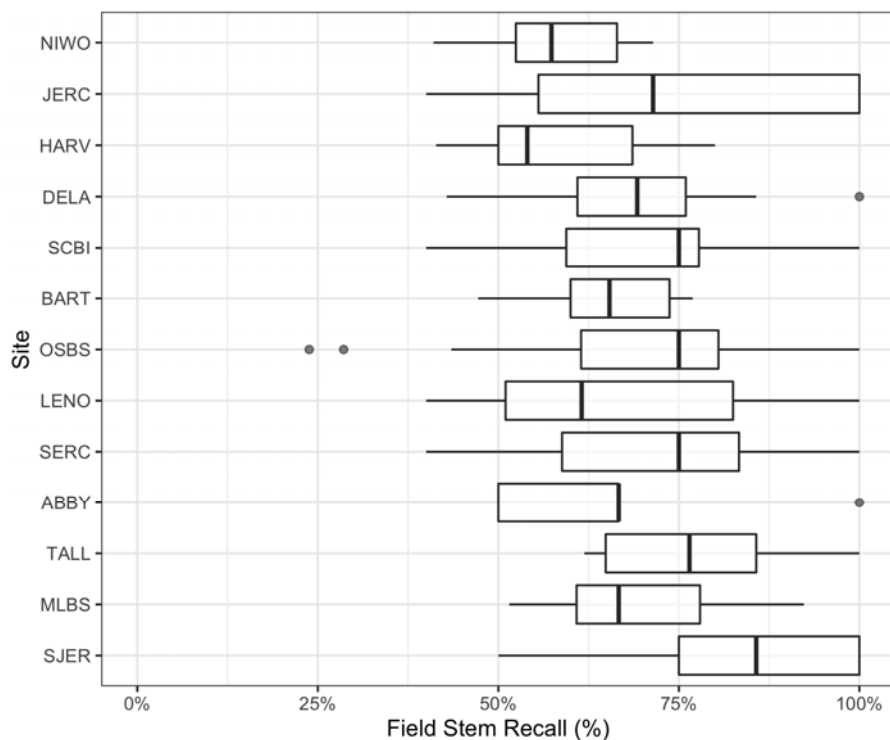
148 forested areas of the NEON sites, rather than in less dense areas of the sites. Areas with less
149 dense forest (e.g., agriculture, suburban areas, and bare ground) are not as common within the
150 NEON field plots used for evaluation and are likely the areas with improved precision from the
151 use of the new LiDAR threshold (Supplementary Material). The 4% increase in precision is
152 therefore likely a lower bound and is worth the trade-off in the minimal drop in recall.



153
154 Figure 4. Precision and recall scores for the algorithm used to create the NEON Crowns Dataset
155 (red points), as well as the DeepForest model from Weinstein et al., (2020a) (blue points).
156 Evaluation is performed on 207 image-annotated images (6926 trees) in the
157 NEONTreeEvaluation dataset (<https://github.com/weecology/NeonTreeEvaluation>).
158

159 We also compared crowns delineated by the algorithm to field-collected stems from
160 NEON's Woody Vegetation Structure dataset. This data product contains a single point for each
161 tree with a stem diameter ≥ 10 cm. We filtered the raw data to only include trees likely to be

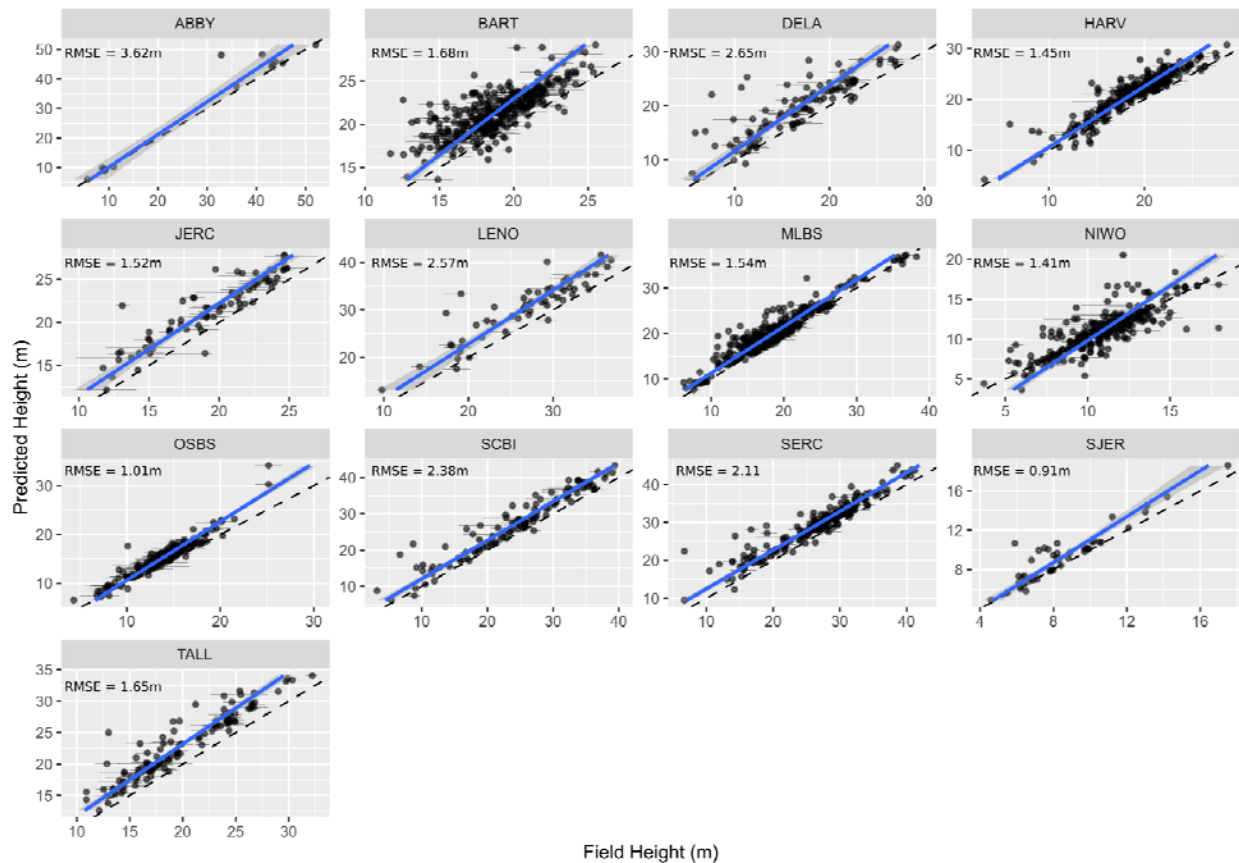
162 visible in the canopy (see Appendix S1). These overstory tree field data help us analyze the
163 performance of our workflow in matching crown predictions to individual trees by scoring the
164 proportion of field stems that fall within a prediction. Field stems can only be applied to one
165 prediction, so if two predictions overlap over a field stem, only one is considered a positive
166 match. This test produces an overall stem recall rate at 69.4%, which is similar to the bounding
167 box recall rate from the image-annotated data (Figure 5). The analysis of stem recall rate is
168 conservative due to the challenge of aligning the field-collected spatial data with the remote
169 sensing data (Appendix S1). We found several examples of good predictions that were counted
170 as false positives due to errors in the position of the ground samples within the imagery.



171
172 Figure 5. Overstory stem recall rate for NEON sites with available field data. Each data point is
173 the recall rate for a field-collected plot. NEON plots are either 40mx40m 'tower' plots with two

174 20x20m subplots, or a single 20mx20m 'distributed' plot. See NEON sampling protocols for
175 details. For site abbreviations see S3.

176 To assess the utility of our approach for mapping forest structure, we compared remotely
177 sensed predictions of maximum tree height to field measurements of tree height of overstory
178 trees using NEON's Woody Plant Vegetation Structure Data. We used the same workflow
179 described in Appendix S1 for determining overstory status for both the stem recall and height
180 verification analysis. Predicted heights showed good correspondence with field-measured
181 heights of reference trees. Using a linear-mixed model with a site-level random effect, the
182 predicted crown height had a Root Mean Squared Error of 1.73m (Figure 6). The relationship is
183 stronger in forests with more open canopies (SJER, OSBS) and predictably more prone to error
184 in forests with denser canopies (BART, MLBS). Given the challenges of measuring tree heights,
185 including the difficulty of measuring tree height in the field, the potential for tree growth between
186 the time of field measurement and image acquisition (often several years), and the automated
187 workflow to designate whether field-collected trees were visible in the canopy, these results
188 suggest that overstory height measures are reasonably accurate across the dataset.



189

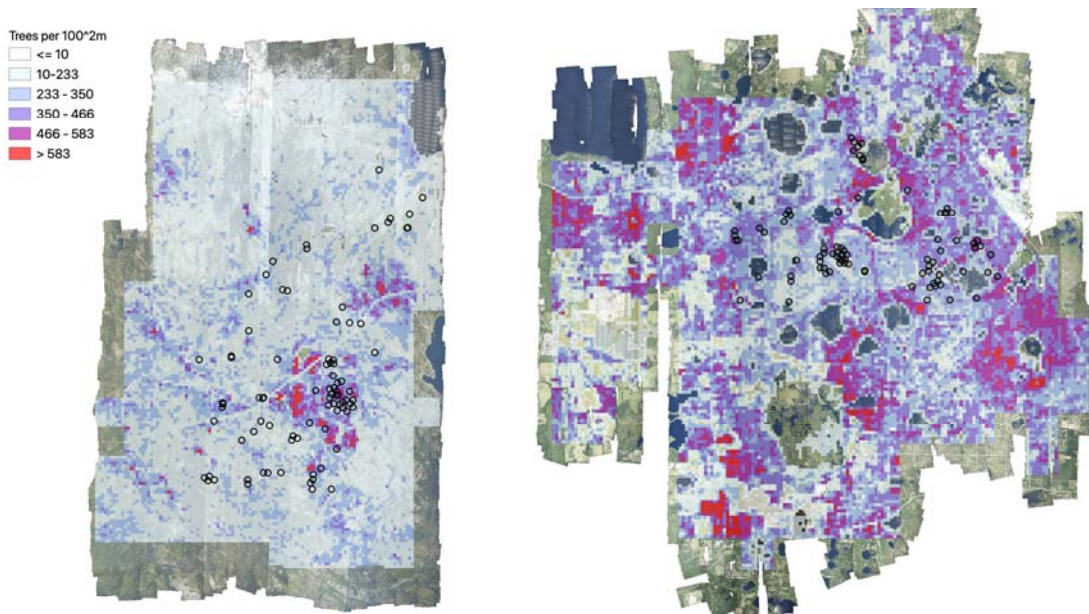
190 Figure 6. Comparison of field and remote sensing measurements of tree heights for 11 sites in
191 the National Ecological Observatory Network. Each point is an individual tree. See text and S1
192 for selection criteria and matching scheme for the field data. The RMSE of a mixed-effects
193 model with a site level random effect is 1.73m.

194 Using the NEON Crowns dataset for individual, landscape and
195 biogeographic scale applications

196 This dataset supports individual-level cross-scale ecological research that has not been
197 previously possible. It provides the unique combination of information spanning the entire United
198 States, with sites ranging from Puerto Rico to Alaska, with continuous individual-level data
199 within sites at scales hundreds of times larger than what is possible using field-based survey

200 methods. At the individual level, high-resolution airborne imagery can inform analysis of critical
201 forest properties, such as tree growth and mortality (Clark et al., 2004), foliar biochemistry
202 (Chadwick and Asner, 2016), and landscape-scale carbon storage (S. J. Graves et al., 2018).
203 Because field data on these properties are measured on individual trees, individual level tree
204 detection allows connecting field data directly to image data. In addition, growth, mortality and
205 changes in carbon storage occur on the scale of individual trees such that detection of individual
206 crowns allows direct tracking of these properties across space and time. While it is possible to
207 aggregate information at the stand level, we believe that individual level data opens new
208 possibilities in large scale forest monitoring and provides richer insights into the underlying
209 mechanisms that drive these patterns.

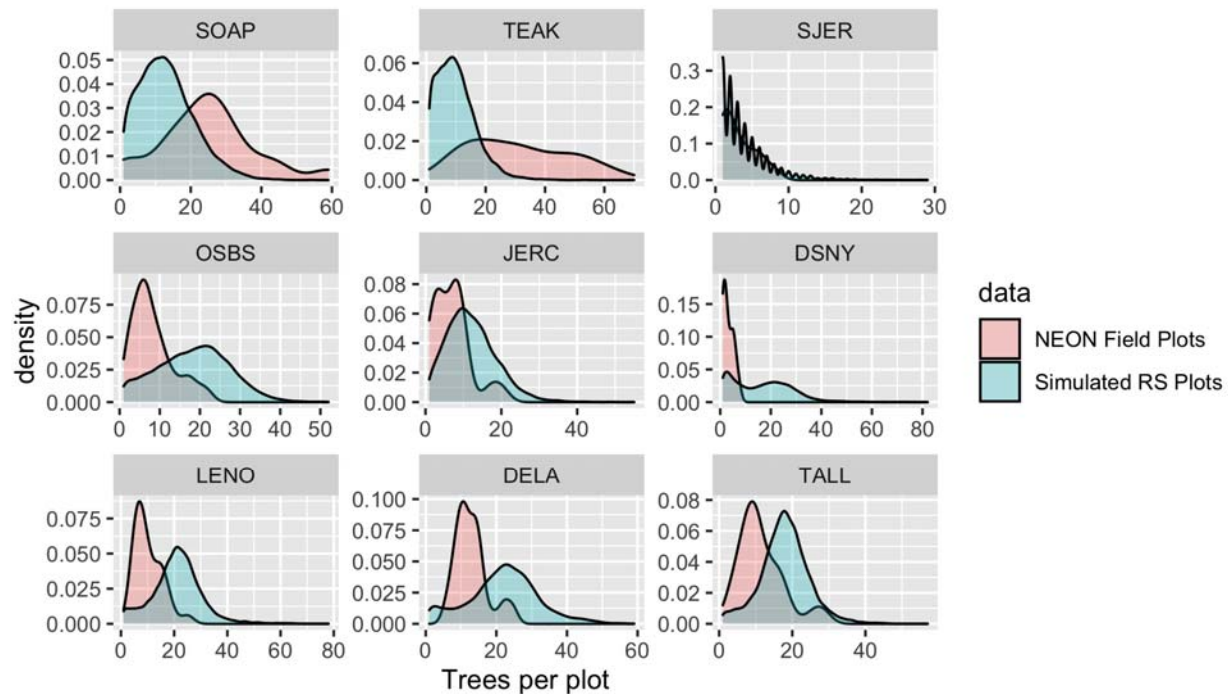
210 At landscape scales, research is often focused on the effect of environmental and
211 anthropogenic factors on forest structure and biodiversity. For example, understanding why tree
212 abundance and biomass vary across landscapes has direct applications to numerous ecological
213 questions and economic implications (e.g. Laubhann et al., 2009). Often this requires sampling
214 at a number of disparate locations and either extrapolation to continuous patterns at landscape
215 scales, or assumptions that the range of possible states of the system are captured by the
216 samples. Using the individual level data from this dataset, we can now produce continuous high-
217 resolution maps across entire NEON sites for enabling landscape scale studies of multiple
218 ecological phenomena (Figure 7). These landscape scale responses can then be combined with
219 high resolution data on natural and anthropogenic drivers (e.g., topography, soils, fire
220 management) to model forest dynamics at broad scales.



221
222 Figure 7. Tree density maps for Teakettle Canyon, California (left) and Ordway Swisher
223 Biological Station, Florida (right). For each 100m² pixel, the total number of predicted crowns
224 were counted. The location of NEON Woody Plant Vegetation sampling plots are shown in black
225 circles.

226 By focusing on detecting individual trees, this approach to landscape scale forest
227 analysis does not require assumptions about spatial similarity, sufficiently extensive sampling,
228 or consistent responses of the ecosystem to drivers across spatial gradients. This is important
229 because the heterogeneity of forest landscapes makes it difficult to use field plot data on
230 quantities such as tree density and biomass to extrapolate inference to broad scales (Marvin et
231 al., 2014). To illustrate this challenge, we compared field-measured tree densities of NEON field
232 plots to estimated densities of 10,000 remotely sensed plots of the same size placed randomly
233 throughout the landscapes across footprints of the airborne data. We attempted to change the
234 Woody Vegetation data as little as possible (i.e. compared to the more refined filtered data in
235 previous analyses) in order to obtain estimates of tree cover in a plot from the field data. To be

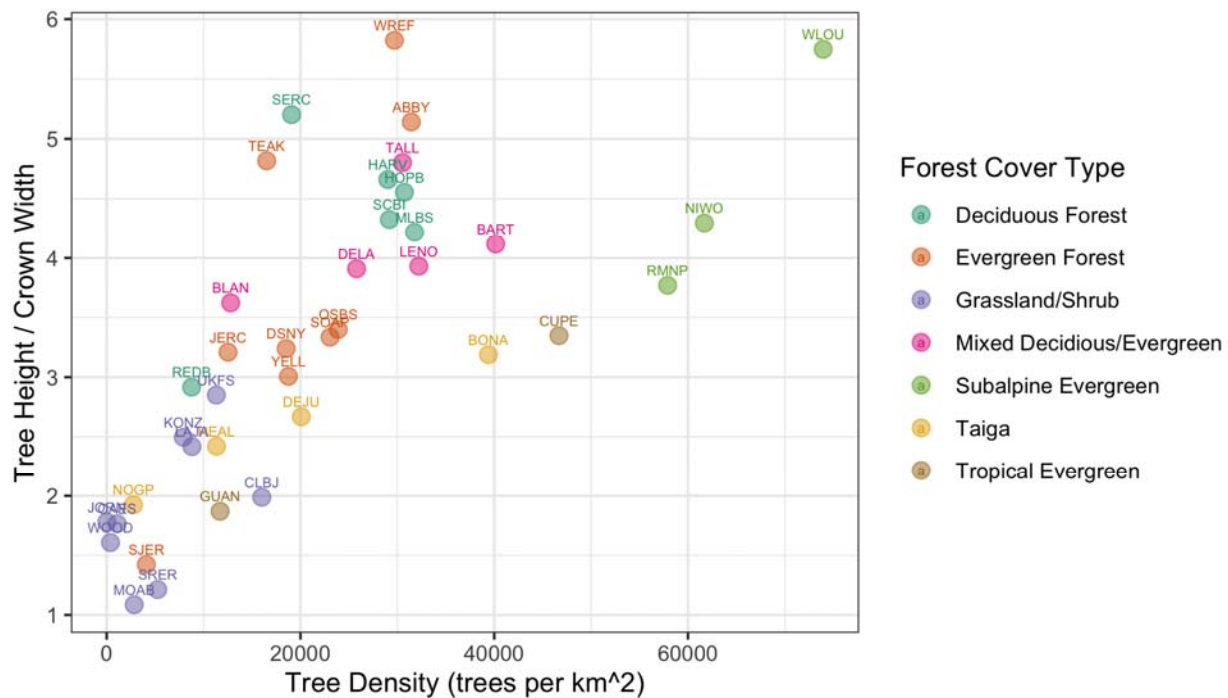
236 included in this analysis, trees needed to have valid spatial coordinates and a minimum height
237 of 3m. Some older data lacked height estimates, in which case we used a minimum dbh
238 threshold of 15cm. In each simulated plot, we then counted the total number of predicted tree
239 crowns to create a distribution of tree densities at the site level (Figure 8). Comparing the field
240 plot tree densities with the distribution from the full site shows deviations for most sites, with
241 NEON field plots exhibiting higher tree densities than encountered on average in the airborne
242 data for some sites (e.g., Teakettle Canyon, CA) and lower tree densities than from remote
243 sensing in others (e.g., Ordway-Swisher Biological Station). While this kind of comparison is
244 inherently difficult due to differing thresholds and filters for data inclusion in field versus remotely
245 sensed data, it highlights that even well stratified sampling of large landscapes as was done
246 with NEON plots (see NEON technical documents for NEON.DP1.10098) can produce differing
247 tree attribute estimates than continuous sampling from remote sensing data. Combining
248 representative field sampling with remote sensing to produce data products like the NEON
249 Crowns dataset provides an approach to addressing this challenge to improve estimations of
250 the abundance, biomass, and size distributions across large geographic areas.



251
252 Figure 8. Comparison of tree counts between the field-collected NEON plots and the predicted
253 plots from the dataset. For the remote sensing data, 10000 simulated 40m² plots were
254 calculated for each site for the full AOP footprint for each year. To mimic NEON sampling, 2
255 quadrants were randomly sampled in each simulated plot. No plots on water, bare ground, or
256 herbaceous land classes were included in the comparison. We selected three sites from three
257 NEON domains to show a sample of sites across the continental US. Both distributed and tower
258 NEON plots were used for these analyses.

259
260 The NEON Crowns dataset supports the assessment of cross-site patterns to help
261 understand the influence of large-scale processes on forest structure at biogeographic scales.
262 For example, ecologists are interested in how and why forest characteristics such as
263 abundance, biomass, and allometric relationships vary among forest types (e.g. Jucker et al.,
264 2017) and how these patterns covary across environmental gradients (Feldpausch et al., 2011).

265 Understanding these relationships is important for inferring controls over forest stand structure,
266 understanding individual tree biology, and assessing stand productivity. By providing
267 standardized data that span near-continental scales, this dataset can help inform the
268 fundamental mechanisms that shape forest structure and dynamics. For example, we can
269 calculate tree allometries (e.g., the ratio of tree height to crown area) on a large number of
270 individual trees across NEON sites and explore how allometry varies with stand density and
271 vegetation type (Figure 9). This example analysis shows a continental-scale relationship, with
272 denser forests exhibiting trees with narrower crowns for the same tree height compared to less
273 dense forests, but also clustering and variation in the relationship within vegetation types. For
274 example, subalpine forests illustrate relationships between tree density and allometry that are
275 distinct from other forest types. By defining both general biogeographic patterns, and deviations
276 therein, this dataset will allow the investigation of factors shaping forest structure at
277 macroecological scales.



279 Figure 9. Individual crown attributes for predictions made at each NEON site. For site
280 abbreviations see S1. Crown area is calculated by multiplying the width and height of the
281 predicted crown bounding box. Crown height is the 99th quantile of the LiDAR returns that fall
282 inside the predicted crown bounding box. Sites are colored by the dominant forest type to
283 illustrate the general macroecological relationship among sites in similar biomes.

284 In addition to these ecological applications, the NEON Crowns dataset can also act as a
285 foundation for other machine learning and computer vision applications in forest informatics,
286 such as tree health assessments, species classification, or foliar trait estimation. In each of
287 these tasks, individual tree delineation is the first step to associate sensor data with ground
288 measurements. However, delineation requires a distinct set of technical background and
289 computational approaches and thus many ecological applications either skip an explicit
290 delineation step entirely (Williams et al., 2020) or apply existing software without detailed
291 exploration of segmentation performance (e.g. Maschler et al., 2018). Ignoring these factors can
292 hamper accurate assessments due to mismatches between sensor data and individuals. While
293 our crown annotations are not perfect, they are specifically tailored to one of the largest and
294 openly accessible datasets that allows pairing individual tree detections with information on
295 species identity, tree health, and leaf traits through NEONs field sampling, and we believe they
296 are sufficiently robust to serve as the basis for broad scale analysis.

297 Limitations and Further Technical Developments

298 An important limitation for this dataset is that it only provides information on sun-exposed tree
299 crowns. It is therefore not appropriate for ecological analyses that depend on accurate
300 characterization of subcanopy trees and the three-dimensional structure of forest stands.
301 Fortunately, a number of the major questions and applications in ecology are primarily

302 influenced by large individuals (Enquist et al., 2020). For example, biomass estimation is largely
303 driven by the canopy in most ecosystems, rather than mid or understory trees that are likely to
304 be missed by aerial surveys. Similarly, habitat classification and species abundance curves can
305 depend on the dominant forest structure that can be inferred from coarse resolution airborne
306 data (Shirley et al., 2013) and could be improved using this dataset. It may be possible to
307 establish relationships between understory and canopy measures using field data that could
308 allow this dataset to be used as part of a broader analysis (Bohlman, 2015). However, this
309 would require significant additional research to validate the potential for this type of approach.

310 An additional limitation is the uncertainty inherent in the algorithmic detection of crowns.
311 While we found good correspondence between image-based crown annotations and those
312 produced by the model for many sites, there remained substantial uncertainty across all sites
313 and reasonable levels of error in some sites. It is important to consider how this uncertainty will
314 influence the inference from research using this and similar datasets. The model is biased
315 towards undersegmentation, meaning that multiple trees are prone to being grouped as a single
316 crown. It is also somewhat conservative in estimating crown extent wherein it tends to ignore
317 small extensions of branches from the main crown. These biases could impact studies of tree
318 allometry and biomass if the analysis is particularly sensitive to crown area. When making
319 predictions for ecosystem features such as biomass, it will be important to propagate the
320 uncertainty in individual crowns into downstream analyses. While confidence scores for
321 individual detections are provided to aid uncertainty propagation, the use of additional ground
322 truth data may also be necessary to infer reliability.

323 One aspect of individual crown uncertainty that we have not addressed is the uncertainty
324 related to image-based crown annotations and measurement of trees in the field (S. Graves et
325 al., 2018). To allow training and evaluating the model across a broad range of forest types, we

326 used image-based crown annotations. This approach assumes that crowns identifiable in
327 remotely sensed imagery accurately reflect trees on the ground. This will not always be the
328 case, as what appears to be a single crown from above may constitute multiple neighboring
329 trees, and conversely, what appears to be two distinct crowns in an image may be two branches
330 of a single large tree (S. Graves et al., 2018). Targeted field surveys will be always needed to
331 validate these predictions and community annotation efforts will allow for assessment of this
332 component of uncertainty.

333 The machine learning workflow used to generate this dataset also has several areas that
334 could be improved for greater accuracy, transferability and robustness. The current model
335 contains a single class 'Tree' with an associated confidence score. This representation prevents
336 the model from differentiating between objects that are not trees and objects for which sufficient
337 training information is not available. For example, the model has been trained to ignore
338 buildings and other vertical structures that may look like trees. However, when confronted by
339 objects data that has never been encountered, it often produces unintuitive results. Examples of
340 objects that did not appear in the training data, and as a result were erroneously predicted as
341 trees, include weather stations, floating buoys, and oil wells. Designing models that can identify
342 outliers, anomalies, and 'unknown' objects is an active area of research in machine learning and
343 will be useful in increasing accuracy in novel environments. In addition, NEON data can
344 sometimes be afflicted by imaging artifacts due to co-registration issues with LiDAR and raw
345 RGB imagery (Appendix S2). This effect can lead to distorted imagery that appears fuzzy and
346 swirled and lead to poor segmentation. An ideal model would detect these areas of poor quality
347 and label them as 'unknown' rather than attempting to detect trees in these regions.

348 Given these limitations, we view this version of the dataset as the first step in an iterative
349 process to improve cross-scale individual level data on trees. Ongoing assessment of these

350 predictions using both our visualization tool and field-based surveys will be crucial to continually
351 identify areas for improvements in both training data and modeling approaches. While iterative
352 improvements are important, the accuracy of the current predictions illustrates that this dataset
353 is sufficiently precise for addressing many cross-scale questions related to forest structure. By
354 providing broad scale crown data we hope to highlight the promising integration between deep
355 learning, remote sensing, and forest informatics, and provide access to the results of this next
356 key step in ecological research to the broad range of stakeholders who can benefit from these
357 data.

358 Acknowledgements

359 We would like to thank NEON staff and in particular Tristan Goulden and Courtney Meier for
360 their assistance and support. This research was supported by the Gordon and Betty Moore
361 Foundation's Data-Driven Discovery Initiative (GBMF4563) to E.P. White and by the National
362 Science Foundation (1926542) to E.P. White, S.A. Bohlman, A. Zare, D.Z. Wang, and A. Singh.
363 The funders had no role in study design, data collection and analysis, decision to publish, or
364 preparation of the manuscript.

365 Literature Cited

- 366 Aubry-Kientz M, Dutrieux R, Ferraz A, Saatchi S, Hamraz H, Williams J, Coomes D, Piboule A,
367 Vincent G. 2019. A Comparative Assessment of the Performance of Individual Tree
368 Crowns Delineation Algorithms from ALS Data in Tropical Forests. *Remote Sens*
369 **11**:1086. doi:10.3390/rs11091086
- 370 Bastin J-F, Rutishauser E, Kellner JR, Saatchi S, Pélissier R, Hérault B, Slik F, Bogaert J, De
371 Cannière C, Marshall AR, Poulsen J, Alvarez-Loyayza P, Andrade A, Angbonga-Basia
372 A, Araujo-Murakami A, Arroyo L, Ayyappan N, de Azevedo CP, Banki O, Barbier N,
373 Barroso JG, Beeckman H, Bitariho R, Boeckx P, Boehning-Gaese K, Brandão H,
374 Brearley FQ, Breuer Ndoundou Hockemba M, Brienen R, Camargo JLC, Campos-Arceiz
375 A, Cassart B, Chave J, Chazdon R, Chuyong G, Clark DB, Clark CJ, Condit R, Honorio
376 Coronado EN, Davidar P, de Haulleville T, Descroix L, Doucet J-L, Dourdain A, Droissart
377 V, Duncan T, Silva Espejo J, Espinosa S, Farwig N, Fayolle A, Feldpausch TR, Ferraz

- 378 A, Fletcher C, Gajapersad K, Gillet J-F, Amaral IL do, Gonmadje C, Grogan J, Harris D,
379 Herzog SK, Homeier J, Hubau W, Hubbell SP, Hufkens K, Hurtado J, Kamdem NG,
380 Kearsley E, Kenfack D, Kessler M, Labrière N, Laumonier Y, Laurance S, Laurance WF,
381 Lewis SL, Libalah MB, Ligt G, Lloyd J, Lovejoy TE, Malhi Y, Marimon BS, Marimon
382 Junior BH, Martin EH, Matius P, Meyer V, Mendoza Bautista C, Monteagudo-Mendoza
383 A, Mtui A, Neill D, Parada Gutierrez GA, Pardo G, Parren M, Parthasarathy N, Phillips
384 OL, Pitman NCA, Ploton P, Ponette Q, Ramesh BR, Razafimahaimodison J-C, Réjou-
385 Méchain M, Rolim SG, Saltos HR, Rossi LMB, Spironello WR, Rovero F, Saner P,
386 Sasaki D, Schulze M, Silveira M, Singh J, Sist P, Sonke B, Soto JD, de Souza CR,
387 Stropp J, Sullivan MJP, Swanepoel B, Steege H ter, Terborgh J, Texier N, Toma T,
388 Valencia R, Valenzuela L, Ferreira LV, Valverde FC, Van Andel TR, Vasque R,
389 Verbeeck H, Vivek P, Vleminckx J, Vos VA, Wagner FH, Warsudi PP, Wortel V, Zagt RJ,
390 Zebaze D. 2018. Pan-tropical prediction of forest structure from the largest trees. *Glob*
391 *Ecol Biogeogr* **27**:1366–1383. doi:10.1111/geb.12803
- 392 Bohlman SA. 2015. Species Diversity of Canopy Versus Understory Trees in a Neotropical
393 Forest: Implications for Forest Structure, Function and Monitoring. *Ecosystems* **18**:658–
394 670. doi:10.1007/s10021-015-9854-0
- 395 Chadwick KD, Asner GP. 2016. Organismic-Scale Remote Sensing of Canopy Foliar Traits in
396 Lowland Tropical Forests. *Remote Sens* **8**:87. doi:10.3390/rs8020087
- 397 Clark DB, Castro CS, Alvarado LDA, Read JM. 2004. Quantifying mortality of tropical rain forest
398 trees using high-spatial-resolution satellite data. *Ecol Lett* **7**:52–59. doi:10.1046/j.1461-
399 0248.2003.00547.x
- 400 Crowther TW, Glick HB, Covey KR, Bettigole C, Maynard DS, Thomas SM, Smith JR, Hintler G,
401 Duguid MC, Amatulli G, Tuanmu M-N, Jetz W, Salas C, Stam C, Piotta D, Tavani R,
402 Green S, Bruce G, Williams SJ, Wiser SK, Huber MO, Hengeveld GM, Nabuurs G-J,
403 Tikhonova E, Borchardt P, Li C-F, Powrie LW, Fischer M, Hemp A, Homeier J, Cho P,
404 Vibrans AC, Umunay PM, Piao SL, Rowe CW, Ashton MS, Crane PR, Bradford MA.
405 2015. Mapping tree density at a global scale. *Nature* **525**:201–205.
406 doi:10.1038/nature14967
- 407 Enquist BJ, Link to external site this link will open in a new window, Abraham AJ, Link to
408 external site this link will open in a new window, J HMB, Yadvinder M, Link to external
409 site this link will open in a new window, Doughty CE, Link to external site this link will
410 open in a new window. 2020. The megabiota are disproportionately important for
411 biosphere functioning. *Nat Commun Lond* **11**.
412 doi:<http://dx.doi.org/10.1038/s41467-020-14369-y>
- 413 Feldpausch TR, Banin L, Phillips OL, Baker TR, Lewis SL, Quesada CA, Affum-Baffoe K, Arets
414 EJMM, Berry NJ, Bird M, Brondizio ES, de Camargo P, Chave J, Djangbletey G,
415 Domingues TF, Drescher M, Fearnside PM, França MB, Fyllas NM, Lopez-Gonzalez G,
416 Hladik A, Higuchi N, Hunter MO, Iida Y, Salim KA, Kassim AR, Keller M, Kemp J, King
417 DA, Lovett JC, Marimon BS, Marimon-Junior BH, Lenza E, Marshall AR, Metcalfe DJ,
418 Mitchard ETA, Moran EF, Nelson BW, Nilus R, Nogueira EM, Palace M, Patiño S, Peh
419 KS-H, Raventos MT, Reitsma JM, Saiz G, Schrodt F, Sonké B, Taedoumg HE, Tan S,
420 White L, Wöll H, Lloyd J. 2011. Height-diameter allometry of tropical forest trees.
421 *Biogeosciences* **8**:1081–1106. doi:10.5194/bg-8-1081-2011
- 422 Graves S, Gearhart J, Caughlin TT, Bohlman S. 2018. A digital mapping method for linking
423 high-resolution remote sensing images to individual tree crowns (preprint). PeerJ
424 Preprints. doi:10.7287/peerj.preprints.27182v1

- 425 Graves SJ, Caughlin TT, Asner GP, Bohlman SA. 2018. A tree-based approach to biomass
426 estimation from remote sensing data in a tropical agricultural landscape. *Remote Sens*
427 *Environ* **218**:32–43. doi:10.1016/j.rse.2018.09.009
- 428 Hansen MC, Potapov PV, Moore R, Hancher M, Turubanova SA, Tyukavina A, Thau D,
429 Stehman SV, Goetz SJ, Loveland TR, Kommareddy A, Egorov A, Chini L, Justice CO,
430 Townshend JRG. 2013. High-Resolution Global Maps of 21st-Century Forest Cover
431 Change. *Science* **342**:850–853. doi:10.1126/science.1244693
- 432 Jucker T, Caspersen J, Chave J, Antin C, Barbier N, Bongers F, Dalponte M, Ewijk KY van,
433 Forrester DI, Haeni M, Higgins SI, Holdaway RJ, Iida Y, Lorimer C, Marshall PL, Momo
434 S, Moncrieff GR, Ploton P, Poorter L, Rahman KA, Schlund M, Sonké B, Sterck FJ,
435 Trugman AT, Usoltsev VA, Vanderwel MC, Waldner P, Wedeux BMM, Wirth C, Wöll H,
436 Woods M, Xiang W, Zimmermann NE, Coomes DA. 2017. Allometric equations for
437 integrating remote sensing imagery into forest monitoring programmes. *Glob Change*
438 *Biol* **23**:177–190. doi:10.1111/gcb.13388
- 439 Laubhann D, Sterba H, Reinds GJ, De Vries W. 2009. The impact of atmospheric deposition
440 and climate on forest growth in European monitoring plots: An individual tree growth
441 model. *For Ecol Manag* **258**:1751–1761. doi:10.1016/j.foreco.2008.09.050
- 442 Marvin DC, Asner GP, Knapp DE, Anderson CB, Martin RE, Sinca F, Tupayachi R. 2014.
443 Amazonian landscapes and the bias in field studies of forest structure and biomass.
444 *Proc Natl Acad Sci* **111**:E5224–E5232. doi:10.1073/pnas.1412999111
- 445 Maschler J, Atzberger C, Immitzer M. 2018. Individual Tree Crown Segmentation and
446 Classification of 13 Tree Species Using Airborne Hyperspectral Data. *Remote Sens*
447 **10**:1218. doi:10.3390/rs10081218
- 448 Puliti S, Breidenbach J, Astrup R. 2020. Estimation of Forest Growing Stock Volume with UAV
449 Laser Scanning Data: Can It Be Done without Field Data? *Remote Sens* **12**:1245.
450 doi:10.3390/rs12081245
- 451 Shirley SM, Yang Z, Hutchinson RA, Alexander JD, McGarigal K, Betts MG. 2013. Species
452 distribution modelling for the people: unclassified landsat TM imagery predicts bird
453 occurrence at fine resolutions. *Divers Distrib* **19**:855–866. doi:10.1111/ddi.12093
- 454 Silva CA, Hudak AT, Vierling LA, Loudermilk EL, O'Brien JJ, Hiers JK, Jack SB, Gonzalez-
455 Benecke C, Lee H, Falkowski MJ, Khosravipour A. 2016. Imputation of Individual
456 Longleaf Pine (*Pinus palustris* Mill.) Tree Attributes from Field and LiDAR Data. *Can J*
457 *Remote Sens* **42**:554–573. doi:10.1080/07038992.2016.1196582
- 458 Weinstein BG, Marconi S, Aubry-Kientz, Méline M, Vincent G, Senyondo H, White E. 2020a.
459 DeepForest: A Python package for RGB deep learning tree crown delineation. *Methods*
460 *Ecol Evol*.
- 461 Weinstein BG, Marconi S, Bohlman S, Zare A, White E. 2019. Individual Tree-Crown Detection
462 in RGB Imagery Using Semi-Supervised Deep Learning Neural Networks. *Remote Sens*
463 **11**:1309. doi:10.3390/rs11111309
- 464 Weinstein BG, Marconi S, Bohlman SA, Zare A, White EP. 2020b. Cross-site learning in deep
465 learning RGB tree crown detection. *Ecol Inform* **56**:101061.
466 doi:10.1016/j.ecoinf.2020.101061
- 467 Williams J, Schönlieb C-B, Swinfield T, Irawan B, Achmad E, Zudhi M, Habibi, Gemita E,
468 Coomes DA. 2020. SLIC-UAV: A Method for monitoring recovery in tropical restoration
469 projects through identification of signature species using UAVs. *ArXiv200606624 Cs*
470 *Stat*.
471
472